JTTEE5 18:593–599
DOI: 10.1007/s11666-009-9358-6
1059-9630/$19.00 © ASM International

Characterization of In-Flight Processing of Alumina Powder Using a DC-RF Hybrid Plasma Flow System at Constant Low Operating Power

H. Nishiyama, M. Onodera, J. Igawa, and T. Nakajima

(Submitted August 6, 2008; in revised form June 17, 2009)

The aim of this study is to provide the optimum operating conditions for enhancing in-flight alumina particle heating as much as possible for particle spheroidization and aggregation of melted particles using a DC-RF hybrid plasma flow system even at constant low operating power based on the thermofluid considerations. It is clarified that the swirl flow and higher operating pressure enhance the particle melting and aggregation of melted particles coupled with increasing gas temperature downstream of a plasma uniformly in the radial direction at constant electrical discharge conditions.

Keywords alumina powder processing, complex interaction, DC-RF hybrid thermal plasma, flow control, particle size distribution, process control

1. Introduction

A DC-RF hybrid plasma flow system, which is combined with a radio frequency inductively coupled plasma (RF-ICP) flow and a direct current (DC) plasma jet, is expected as one of the next-generation thermal plasma system because it has weak back flow, large high-temperature volume, long plasma flame, and high enthalpy (Ref 1, 2). Therefore, it is very important to investigate the optimum operating inlet flow conditions for in-flight powder melting processes using a DC-RF hybrid plasma flow system even at constant low operating power without changing any DC and RF power level and RF frequency to increase the process and energy efficiencies from the stand point of flow control (Ref 3-6). This is because there are complex and strong interactions among ICP discharge, DC plasma jet, and in-flight powders, furthermore, difficulty in fine control of a few micro size powder feeding. Although there are a few papers on modeling of DC-RF sources (Ref 7, 8), the integrated correlation among plasma flow characteristics, in-flight particle behavior, and processed particle properties has not been clarified experimentally in detail (Ref 9-12).

In this study, the effects of operating pressure, swirl flow, quenching gas flow rate and quench gas composition on gas temperature downstream of a plasma, particle velocity, and particle temperature are experimentally clarified for a DC-RF hybrid plasma flow system at constant low operating power. Furthermore, particle size distribution and morphology of in-flight-processed alumina powder are also clarified correlating to the various kinds of operating flow conditions based on our previous thermofluid considerations (Ref 9). The final objective is to provide the optimum operating conditions for enhancing in-flight powder heating as much as possible for spheroidization and aggregation of melted powders using a DC-RF hybrid plasma flow system even at constant low operating power without changing any electrical conditions by parametric approach (Ref 13).

H. Nishiyama, M. Onodera, J. Igawa, and **T. Nakajima**, Institute of Fluid Science, Tohoku University, 2-1-1 Katahira, Aoba-ku, Sendai 980-8577, Japan. Contact e-mail: nishiyama@ifs.tohoku.ac.jp.

2. Experimental Setup and Procedure

Figure 1 shows a schematic illustration of a DC-RF hybrid plasma flow system for in-flight powder processing. A detailed schematic illustration of a DC-RF hybrid plasma torch is also shown in Fig. 2 for sufficient clear

Nomenclature

d_p	particle diameter (μm)
p	operating pressure (kPa)
Q_c	central gas flow rate (Nℓ/min)
$Q_{carrier}$	particle carrier gas flow rate (Nℓ/min)
Q_q	quench gas flow rate (Nℓ/min)
Q_{sh}	sheath gas flow rate (Nℓ/min)
Q_{sw}	swirl gas flow rate (Nℓ/min)
T_g	gas temperature (K)
T_p	particle temperature (K)
V_p	particle velocity (m/s)

understanding of the inlet flow conditions. The anode nozzle is copper and cathode is copper-tungsten with 3 mm diameter in a DC torch. The outer diameter of DC torch and inner quartz tube are 38 and 44 mm, respectively. The inner diameter of RF coil is 64 mm and its inclination is 6°. Three turn coils are located 15, 25, and 35 mm from a DC torch exit. RF power supplied to the RF induction coil is 6.6 kW, 4 MHz, and DC power is 1 kW, respectively. The working gas for plasma flow is argon, and quench gas is argon or nitrogen. The operating pressure is 33 and 53 kPa. The sheath gas is passed axially downward along the inner quartz tube wall for cooling the wall. The swirl gas is injected tangentially from opposing two holes at the DC torch inlet coupled with sheath gas. The central gas is introduced along the outside of cathode to produce the plasma jet. The flow rates of sheath gas Q_{sh} without swirl or with Q_{sw}, central gas Q_c, and quench gas Q_q are 20, 3, and 0-50 Nℓ/min, respectively. When the powder is injected to the plasma flow, a carrier gas is also injected around the core of DC torch as shown in Fig. 2. The powder carrier gas $Q_{carrier}$ is 0.5 Nℓ/min for particle trajectory velocimetry (PTV) method and 0.8 Nℓ/min for in-flight powder processing. The quench gas is passed from the tube ring with 12 holes of 2 mm diameter which is located 130 mm downstream from a torch exit as shown in Fig. 1. Only alumina particles (Ref 14-17) with 4 μm are supplied at 0.2 g/min as the initial precursors for easiest powder melting at constant low operating power, although control of constant small amount of a few micron powder feeding is difficult due to the particle aggregation in a feeding tube with 2 mm in diameter. The melting temperature of alumina is 2319 K.

The gas temperature is measured by thermoresistant W-Re thermocouple at $z = 196$ mm without a correction of radiation loss and thermal conduction loss from the thermocouple because the emissivity and thermal conductivity of the surface of ceramic coating thermocouple can not be exactly evaluated. However, the range of experimental uncertainty lies from 14 to 57% for directly measured temperature of 1000 K, when considering both assumed losses. The in-flight particle temperature and particle velocity for alumina with 15 μm are also measured by two-wave length pyrometry at 700 and 800 nm and PTV method, respectively, in a spray watch system at $z =$ 196 mm (Ref 18). The measurement principle of PTV is that particle velocity can be obtained by the ratio of flight distance of targeted particle with pulsed laser reflection in the photo image to the exposure time of CCD camera. Furthermore, the in-flight processed powders are collected only at the bottom of a system, which is 870 mm

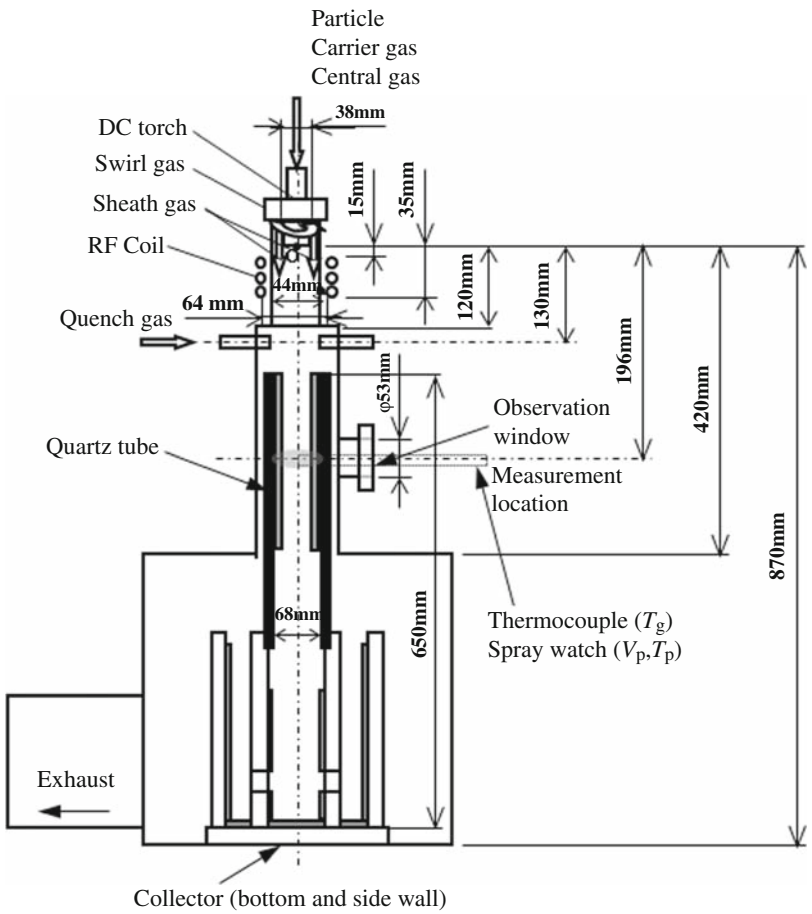

Fig. 1 Schematic illustration of a DC-RF hybrid plasma flow system for in-flight powder processing

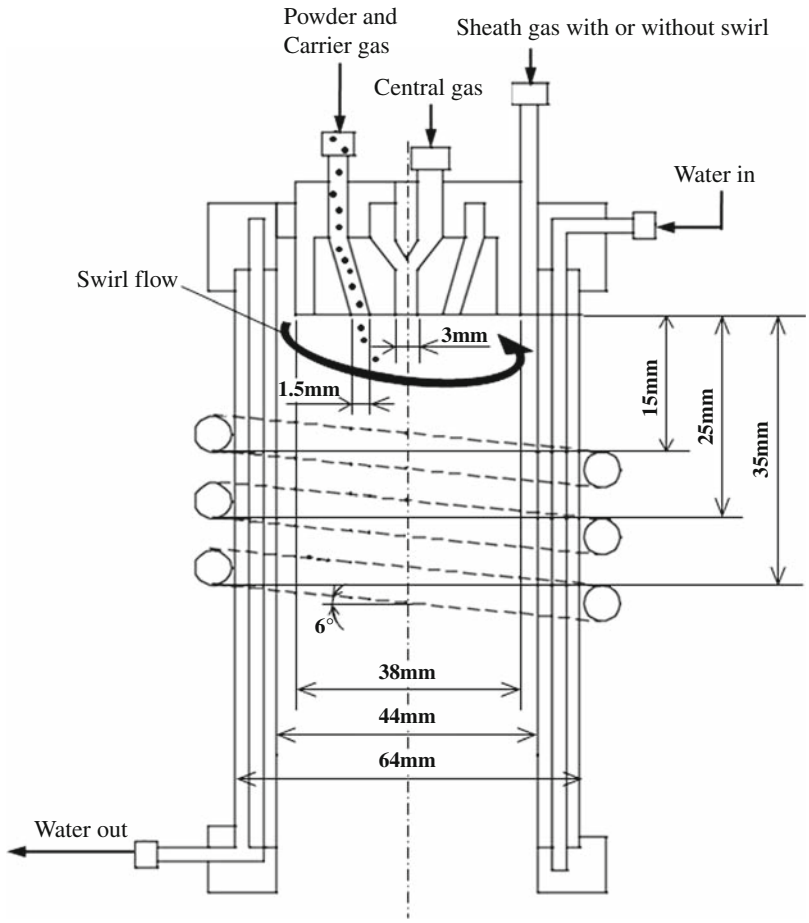

Fig. 2 Schematic illustration of a DC-RF hybrid plasma torch

downstream from a DC nozzle exit. The particle size distribution is measured by particle size analyzer (MT3000, Microtrac Inc.) after 90 s ultrasonic treatment. The particle size and particle morphology are characterized by scanning electron microscope (SEM, S4100, Hitachi).

3. Experimental Results and Discussion

Figure 3(a) to (d) shows photos of plasma flow view from observation window for various operating conditions without powder injection. The exposure time of camera is 1 ms. Unfortunately, the high-speed imaging for plasma behavior is not shown in this study. The operating conditions are as follows:

(a) $p = 53$ kPa, $Q_c = 3$ Nℓ/min, $Q_{sw} = 20$ Nℓ/min, $Q_{q,Ar} = 0$ Nℓ/min
(b) $p = 33$ kPa, $Q_c = 3$ Nℓ/min, $Q_{sw} = 20$ Nℓ/min, $Q_{q,Ar} = 0$ Nℓ/min
(c) $p = 33$ kPa, $Q_c = 3$ Nℓ/min, $Q_{sw} = 20$ Nℓ/min, $Q_{q,Ar} = 50$ Nℓ/min
(d) $p = 33$ kPa, $Q_c = 3$ Nℓ/min, $Q_{sw} = 20$ Nℓ/min, $Q_{q,N_2} = 5$ Nℓ/min

A plasma flame elongates downstream at low operating pressure in Fig. 3(b) compared with that in Fig. 3(a). The plasma is still stable and it has clear flame even for large quench flow rate of argon in Fig. 3(c), but plasma volume is small with sharp-edged plasma tail. Furthermore, plasma itself becomes visibly unstable with fluctuating emission and moving of plasma flame, detected through eye observation for giving even small quench flow rate of nitrogen gas in Fig. 3(d). This unstable plasma behavior can also be observed by increasing the sheath gas flow rates in the previous study (Ref 19). This is because large energy is consumed in the RF coil region by dissociation and ionization of injected quench nitrogen gas, which returns upstream along the quartz tube wall from the quench location toward the RF coil discharge tail due to the back flow along the RF tube wall without powder injection (Ref 8, 9).

Figure 4(a) and (b) shows the radial distribution of gas temperature at $z = 196$ mm and $p = 33$ and 53 kPa without swirl to clarify the effects of argon gas quench flow rate and operating pressure on the gas temperature decrease in the downstream. Unfortunately, there is lack of

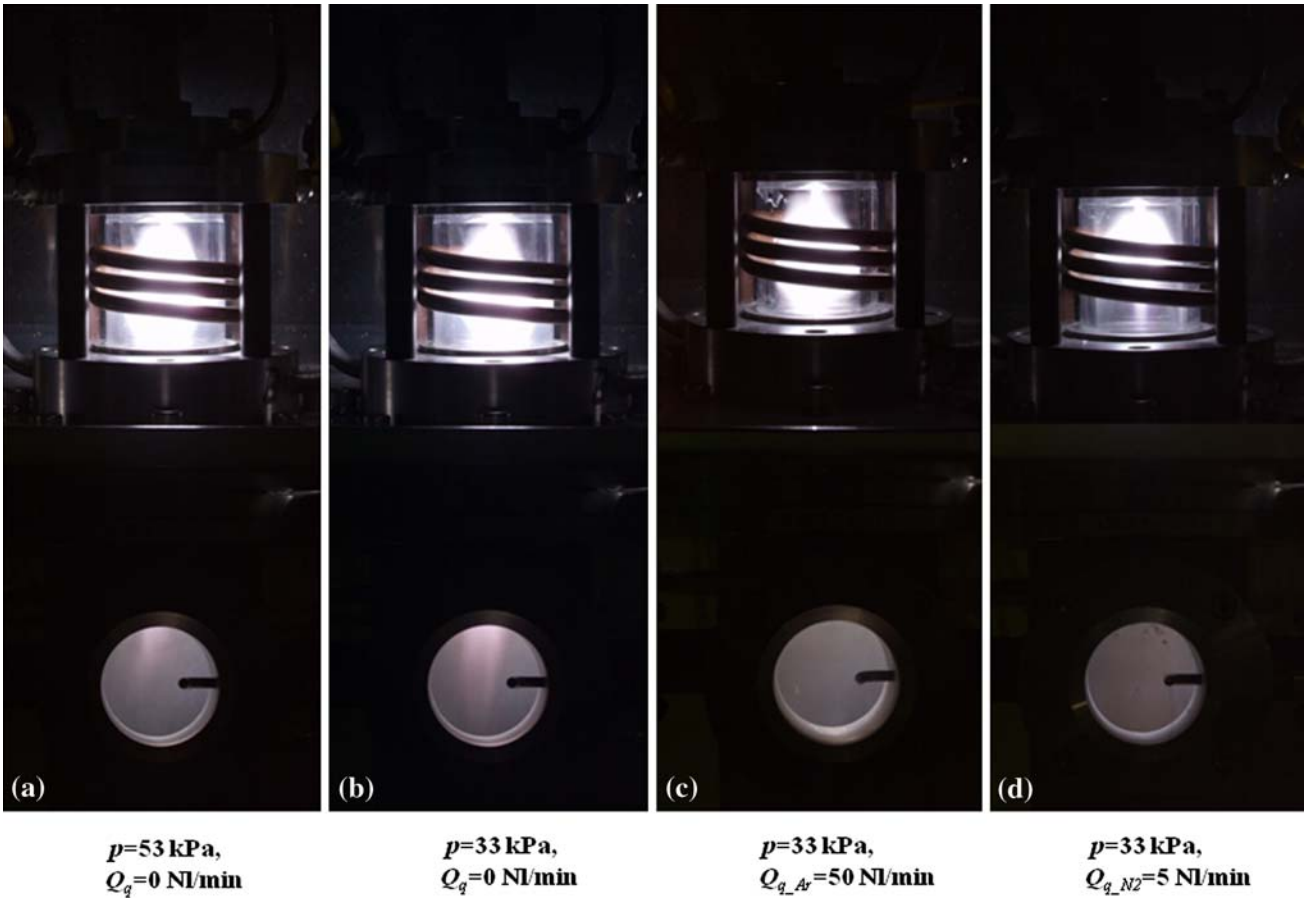

Fig. 3 (a-d) Plasma photos for various operating conditions

experimental data less than 15 mm due to the thermal fatigue of thermocouple and the influence of many electrons in a DC jet at a high operating pressure as shown in Fig. 4(b). The decrease in the gas temperature downstream of a plasma ranges from 15 to 50% with increase in the quench gas flow rates more than 20 Nℓ/min. The gas temperature at $p = 53$ kPa in Fig. 4(b) is about 20% higher especially for quench flow rates of 50 Nℓ/min than that at $p = 33$ kPa in Fig. 4(a) due to the active collision between the high energetic electrons and heavy particles in a higher operating pressure. This means that the effect of quench gas flow rate on gas temperature decrease is large at lower operating pressure in the present experimental conditions.

Figure 5 shows the radial distributions of gas temperature at $z = 196$ mm to clarify the swirl effect. There is a large difference of temperature between core region and near tube wall without swirl flow in Fig. 4(a). On the other hand, there is a small difference of gas temperature between core and near tube wall showing relatively uniform in the radial direction and also decrease in temperature with quench gas being smaller than that without swirl as shown in Fig. 5. This is because the hot core of DC jet diffuses toward the quartz tube wall and is mixed with high-temperature region of ICP by centrifugal force due to the swirling sheath gas.

Figure 6 shows the radial distributions of gas temperature downstream of a plasma to clarify the effect of nitrogen quench gas. When even small amount of nitrogen gas is injected more than 5 Nℓ/min as a quench gas, plasma flow becomes unstable and disappears due to only dissociation of nitrogen as shown in Fig. 3(d). Since there is a upper limitation of injected nitrogen quench gas flow rate for producing a stable plasma flow due to only dissociation of reversing nitrogen gas flow at a low electric power, quenching effect by small amount of nitrogen gas is relatively small in this system.

Figure 7(a) and (b) shows the correlation between in-flight particle velocity and particle temperature without and with swirl for various quench gas flow conditions and operating pressure at $z = 196$ mm. The particle velocity decreases at $p = 53$ kPa due to smaller plasma velocity and larger particle drag independent of swirl flow. But, the particle velocity generally increases with large argon quench gas flow rate at $p = 53$ kPa due to the increase in momentum transfer from quench gas flow. The particle temperature shows nearly 2000 K for both of argon quench gas flow rates and operating pressure due to uniform gas mixing and particle heating by swirl flow as shown in Fig. 7(b). On the other hand, both the particle velocity and particle temperature show scattered

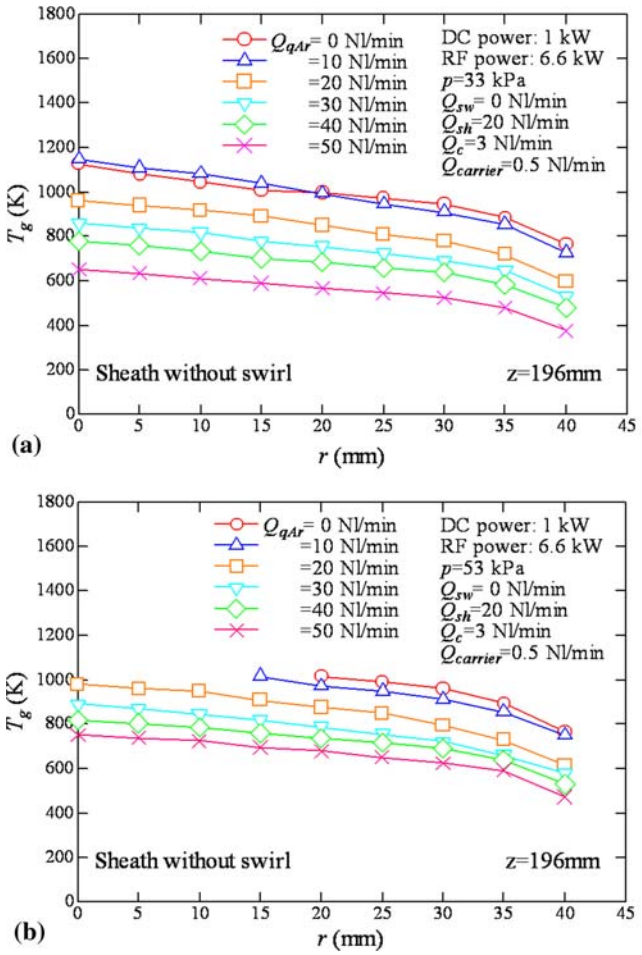

Fig. 4 (a, b) Radial distributions of gas temperature with operating pressure

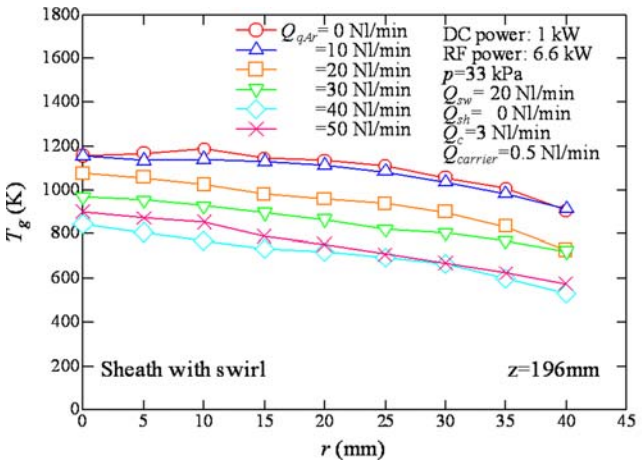

Fig. 5 Radial distributions of gas temperature with swirl

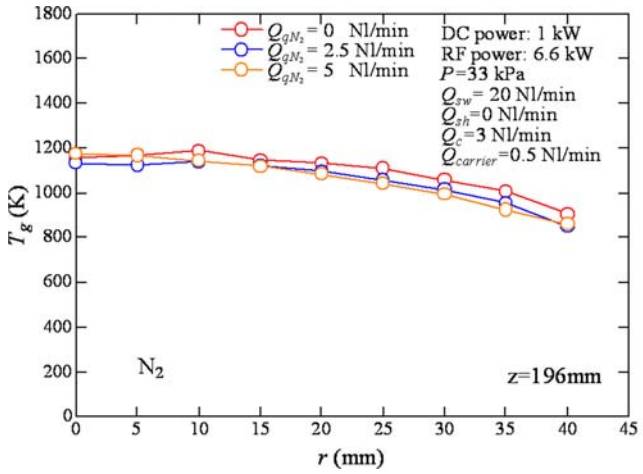

Fig. 6 Radial distributions of gas temperature with nitrogen quench gas

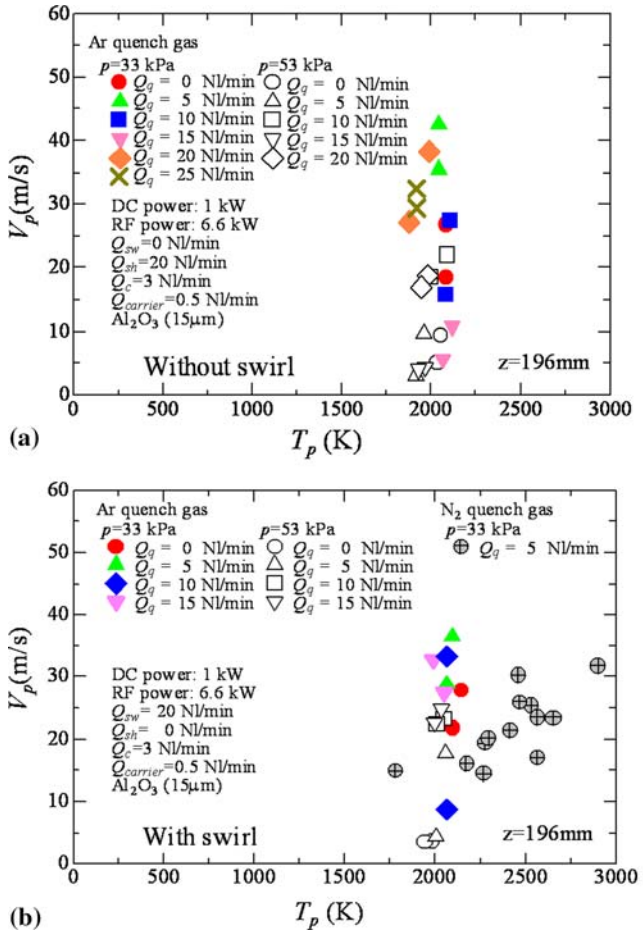

Fig. 7 (a, b) Correlation between particle temperature and particle velocity for various operating conditions

distributions for nitrogen quench gas injection due to nonuniform particle trajectory and particle heating in an unstable plasma flow condition with dissociation of reversing nitrogen gas flow and momentum transfer of heavy nitrogen gas as shown in Fig. 3(d).

Figure 8(a) to (c) shows the typical Al_2O_3 SEM micrographs of initial precursor and in-flight processed

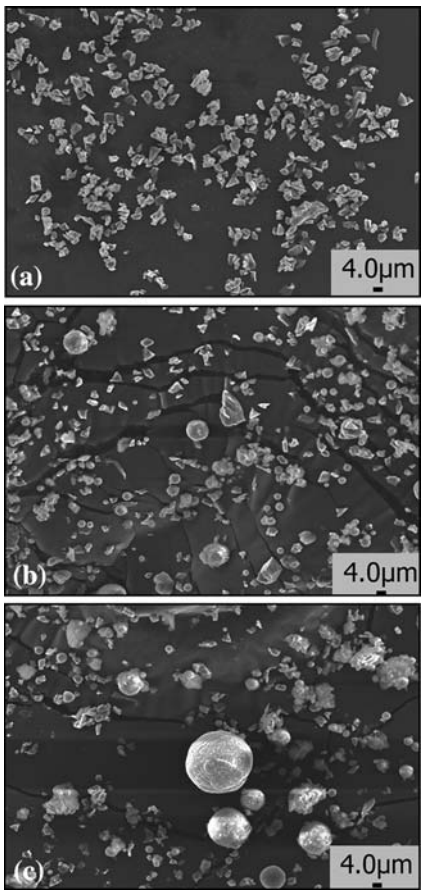

Fig. 8 (a-c) SEM micrographs of initial precursor and in-flight processed alumina powders

powders under operating pressure of 33 kPa without swirl and quench gas and under operating pressure of 53 kPa with swirl and without quench gas, respectively. The morphology geometry of initial precursor is polygonal in Fig. 8(a). Some of processed powders are spherical due to the surface tension of fusion particle as shown in Fig. 8(b), although mean spheroidization rate is about 35% at the system bottom, which is located 870 mm downstream from a DC torch exit. The spheroidization rate is defined as the ratio of number of spherical particles to that of the total particles collected at the system bottom after plasma treatment in the SEM image. The aggregation and combination of partially melted particles are observed forming eight times larger particle compared with raw alumina powder, for example, in the case of swirl and higher operating pressure in Fig. 8(c).

Figure 9 shows the particle size distributions to clarify the effects of swirl flow, operating pressure, and quench gas for four cases, when the processed powders are collected at the system bottom. The reference condition for case 1 is $P_{DC} = 1$ kW, $Q_{sh} = 20$ Nℓ/min, $p = 33$ kPa, and $Q_{q,Ar} = 0$ Nℓ/min. The dashed line shows the precursor particle size distribution before plasma treatment of which mean diameter is 4 μm. The sum of powder weights collected at the bottom in all the four cases is smaller than

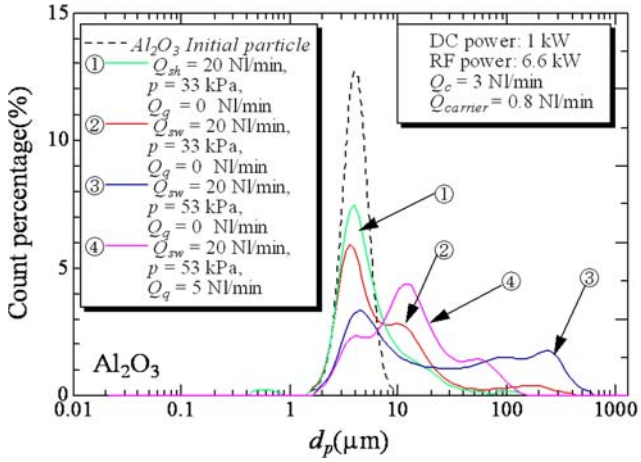

Fig. 9 Particle size distributions for various operating conditions

that of the raw alumina powder fed into the apparatus. This means that the particle collection ratio is below 1 in all the four cases. This is because the partial evaporation of particle and particle deposition onto the side wall and other inside walls have occurred. In case 1, the particle size increases only forming particles between 10 and 30 μm due to a small amount of particle surface melting and spheroidization as shown in Fig. 8(b). In case 2 with swirl, the count percentage increases still more ranging from 10 to 30 μm due to melting and subsequent particle aggregation by active thermal diffusion as shown in Fig. 5. In case 3 with high operating pressure, a wide spread of particle size distribution forming particles between 10 and 300 μm is shown, and some particle diameter increases considerably due to active melting with long residence time of particle in a high-temperature region (Ref 11) and subsequent active aggregation and combination of partially melted particles as shown in Fig. 7(b) and 8(c). This case shows the optimum operating condition to make a bigger size of particles with aggregation. In case 4 with quench gas injection, the count percentage of large aggregated particle more than 100 μm decreases considerably since particle melting and aggregation are suppressed by quenching effect.

4. Conclusions

An experimental study is conducted to obtain the optimum operating flow conditions for in-flight alumina powder processing in particle size and morphology controls using a DC-RF hybrid plasma flow system at constant low operating power based on thermofluid considerations. The obtained results are as follows:

1. The plasma flame elongates downstream at low operating pressure. The plasma volume is small and plasma itself becomes unstable when even small amount of nitrogen quench gas is injected in the downstream of a plasma.

2. The gas temperature downstream of a plasma becomes radially uniform by giving swirl gas. The gas temperature considerably decreases with increase in the argon gas quench flow rate more than 20 Nℓ/min at low operating pressure without swirl, but increases at high operating pressure.
3. The particle velocity decreases at high operating pressure due to larger drag force resulting in larger in-flight residence time. The particle temperature is nearly 2000 K both for operating pressure and quench gas flow rate with swirl flow. When nitrogen quench gas is injected, particle velocity and particle temperature show scattered distribution due to the plasma flow fluctuation.
4. In the in-flight alumina powder processing, melting amount of powders increases with increase in operating pressure and swirl flow, forming spherical particles and larger aggregated particles. But, particle aggregation is suppressed by quenching gas in the downstream of a plasma.
5. The swirl gas flow and higher operating pressure are considerably effective key operating parameters for in-flight powder processing at constant low electric power operation of a complex DC-RF hybrid plasma flow system.

Acknowledgments

We would like to extend our sincere thanks to Dr. K. Kawajiri with National Institute of Advanced Industrial Science and Technology and Assistant Prof. H. Takana with Institute of Fluid Science, Tohoku University for their valuable discussions and to Mr. K. Katagiri with our institute for his technical support. This research was partially supported by Grant-in-Aid for Scientific Research (A) (2005-2007) from the Japan Society for the Promotion of Science and a 21st Century COE program Grant (2003-2007) of the International COE of Flow Dynamics from the Ministry of Education, Culture, Sports, Science and Technology.

References

1. T. Yoshida, T. Tani, H. Nishimura, and K. Akashi, Characterization of a Hybrid Plasma and Its Application to Chemical Synthesis, *J. Appl. Phys.*, 1983, **54**(2), p 640-646
2. K.S. Kim, J.H. Seo, J.S. Nam, W.T. Ju, and S.H. Hong: Production of Hydrogen and Carbon Black by Methane Decomposition Using DC-RF Hybrid Thermal Plasmas, *IEEE Trans. Plasma Sci.*, 2005, **33**(2), p 813-823
3. L. Jia and F. Gitzhofer, Collection of Nano-powders Generated by Radio Frequency (RF) Plasma Spray Synthesis (PSS) Processing, Using a Sampling Probe, *Proceedings of the 17th International Symposium on Plasma Chemistry*, J. Mostaghimi, T.W. Coyle, V.A. Pershin, H.R. Salimi Jazi, Ed., 7-12 Aug 2005 (Toronto), 2005, CD-ROM
4. Y. Kousaka, T. Nomura, M. Nishimoto, and E. Tenjiku, Experimental Studies on Gas-phase Nucleation and the Effect of Seed Particles on Homogeneous Nucleation Suppression, *J. Aerosol Sci.*, 2000, **31**(5), p 519-530
5. S.V. Joshi, Q. Liang, J.Y. Park, and J.A. Batdorf, Effect of Quenching Conditions on Particle Formation and Growth in Thermal Plasma Synthesis of Fine Powders, *Plasma Chem. Plasma Process.*, 1990, **10**(2), p 339-358
6. O. Kovářík, X. Fan, and M. Boulos, In Flight Properties of W Particles in an Ar-H_2 Plasma, *J. Therm. Spray Technol.*, 2007, **16**(2), p 229-237
7. J.W. McKelliget and N. El-Kaddah, Modeling of Materials Synthesis in Hybrid Plasma Reactors: Production of Silicon by Thermal Decomposition of $SiCI_4$, *Metall. Trans. B*, 1990, **21**(3), p 589-598
8. J.H. Seo, J.M. Park, and S.H. Hong, Influence of DC Arc Jets on Flow Fields Analyzed by an Integrated Numerical Model for a DC-RF Hybrid Plasma, *Plasma Sources Sci. Technol.*, 2008, **17**(2), p 025011
9. K. Kawajiri, T. Sato, and H. Nishiyama, Experimental Analysis of a DC-RF Hybrid Plasma Flow, *Surf. Coat. Technol.*, 2003, **171** (1-3), p 134-139
10. K. Kawajiri, K. Ramachandran, and H. Nishiyama, Statistical Optimization of a DC-RF Hybrid Plasma Flow System for In-flight Particle Treatment, *Int. J. Heat Mass Transfer*, 2005, **48**(1), p 183-190
11. K. Kawajiri and H. Nishiyama, In-Flight Particle Characteristics in a DC-RF Hybrid Plasma Flow System, *Thin Solid Films*, 2006, **506-507**, p 660-664
12. R. Ye, J.-G. Li, and T. Ishigaki, Controlled Synthesis of Alumina Nanoparticles Using Inductively Coupled Thermal Plasma with Enhanced Quenching, *Thin Solid Films*, 2007, **515**(9), p 4251-4257
13. H. Nishiyama, M. Onodera, J. Igawa, and T. Nakajima, Evaluation of In-Flight Particle Process Using a Small Power DC-RF Hybrid Plasma Flow System, *Proceedings of the 18th International Symposium on Plasma Chemistry*, K. Tachibana, O. Takai, K. Ono, and T. Shirafuji, Ed., 26-31 Aug 2007 (Kyoto), 2007, CD-ROM
14. Y. Li and T. Ishigaki, Thermodynamic Analysis of Nucleation of Anatase and Rutile from TiO_2 Melt, *J. Cryst. Growth*, 2002, **242**(3-4), p 511-516
15. Y. Li and T. Ishigaki, Controlled One-Step Synthesis of Nanocrystalline Anatase and Rutile TiO_2 Powders by In-Flight Thermal Plasma Oxidation, *J. Phys. Chem. B*, 2004, **108**, p 15536-15542
16. T. Ihara, M. Miyoshi, M. Ando, S. Sugihara, and Y. Iriyama, Preparation of a Visible-Light-Active TiO_2 Photocatalyst by RF Plasma Treatment, *J. Mater. Sci.*, 2001, **36**(17), p 4201-4207
17. J.G. Li, H. Kamiyama, X.H. Wang, Y. Moriyoshi, and T. Ishigaki, TiO_2 Nanopowders via Radio-frequency Thermal Plasma Oxidation of Organic Liquid Precursors: Synthesis and Characterization, *J. Eur. Ceram. Soc.*, 2006, **26**, p 423-442
18. X. Chen and E. Pfender, Behavior of Small Particles in a Thermal Plasma Flow, *Plasma Chem. Plasma Process.*, 1983, **3**(3), p 351-366
19. P. Buchner, H. Schubert, J. Uhlenbusch, and M. Weiss, Diagnostics of an RF Plasma Flash Evaporation Process Using the Monochromatic Imaging Technique, *Plasma Chem. Plasma Process.*, 2001, **21**(1), p 1-21